ORIGINAL ARTICLE

OPO   THE COLLEGE OF OPTOMETRISTS

Prediction of corneal back surface power – Deep learning algorithm versus multivariate regression

Achim Langenbucher[1] | Nóra Szentmáry[2,3] | Alan Cayless[4] | Johannes Weisensee[1] | Jascha Wendelstein[5] | Peter Hoffmann[6]

[1]Department of Experimental Ophthalmology, Saarland University, Homburg/Saar, Germany

[2]Dr. Rolf M. Schwiete Center for Limbal Stem Cell and Aniridia Research, Saarland University, Homburg/Saar, Germany

[3]Department of Ophthalmology, Semmelweis-University, Budapest, Hungary

[4]School of Physical Sciences, The Open University, Milton Keynes, UK

[5]Department of Ophthalmology, Johannes Kepler University, Linz, Austria

[6]Augen- und Laserklinik Castrop-Rauxel, Castrop-Rauxel, Germany

Correspondence
Achim Langenbucher, Department of Experimental Ophthalmology, Saarland University, Homburg/Saar, Germany.
Email: achim.langenbucher@uks.eu

Abstract

Background: The corneal back surface is known to add some against the rule astigmatism, with implications in cataract surgery with toric lens implantation. This study aimed to set up and validate a deep learning algorithm to predict corneal back surface power from the corneal front surface power and biometric measures.

Methods: This study was based on a large dataset of IOLMaster 700 measurements from two clinical centres. $N = 19{,}553$ measurements of 19,553 eyes with valid corneal front (CFSPM) and back surface power (CBSPM) data and other biometric measures. After a vector decomposition of CFSPM and CBSPM into equivalent power and projections of astigmatism to the 0°/90° and 45°/135° axes, a multi-output feedforward neural network was derived to predict vector components of CBSPM from CFSPM and other measurements. The predictions were compared with a multivariate linear regression model based on CFSPM components only.

Results: After pre-conditioning, a network with two hidden layers each having 12 neurons was derived. The dataset was split into training (70%), validation (15%) and test (15%) subsets. The prediction error (predicted corneal back surface power CBSPP – CBSPM) of the network after training and crossvalidation showed no systematic offset, narrower distributions for CBSPP – CBSPM and no trend error of CBSPP – CBSPM vs. CBSPM for any of the vector components. The multivariate linear model also showed no systematic offset, but broader distributions of the prediction error components and a systematic trend of all vector components vs. CFSPM components.

Conclusion: The neural network approach based on CFSPM vector components and other biometric measures outperforms the multivariate linear model in predicting corneal back surface power vector components. Modern biometers can supply all parameters required for this algorithm, enabling reliable predictions for corneal back surface data where direct corneal back surface data are unavailable.

KEYWORDS
biometry, corneal back surface power, deep learning algorithm, feedforward multi-output network, neural network, posterior corneal astigmatism

BACKGROUND

Over the last two decades, research has investigated the effect of corneal back surface power on the imaging properties of the eye.[1,2] Especially in biometry and intraocular lens power calculation before cataract surgery, the corneal back surface is widely discussed as a relevant parameter, as well as after keratorefractive surgery.[3–5] Modern anterior segment tomographers provide reliable data on the corneal front and back surface curvature[1,6–8] and central corneal thickness (CCT) as well as the dimensions of the anterior chamber and crystalline lens which is used in several newer generation lens power calculation strategies. However, most biometers such as the IOLMaster 500 (Carl-Zeiss-Meditec, zeiss.com), the LenStar 900 (Haag-Streit, haag-streit.com) or the OA-2000 (Tomey, tomey.com) do not provide measurements of the corneal back surface.

Especially in the context of toric lens calculation, it is widely discussed that the corneal back surface curvature does not follow a fixed ratio of anterior to posterior curvature, as assumed by keratometers which measure corneal front surface curvature and convert this to corneal power using an assumed refractive index.[3,4,9–12] The corneal back surface astigmatism shows some against the rule astigmatism which has to be considered during toric lens power calculations in order to yield the correct refractive results after surgery.[13]

With the classical Javal's rule[14,15] we already know that there exists some discrepancy between keratometric astigmatism and the total ocular astigmatism, which could be due to lenticular or corneal back surface astigmatism. For clinical purposes, Javal's rule is generalised with Grosvenor's simplification.[16] Whereas lenticular astigmatism cannot be currently measured *in vivo* with sufficient accuracy, high-resolution anterior segment tomographers, mostly based on swept source optical coherence tomography (SS-OCT) do quantify corneal back surface curvature.[10,12,17] In the last decade, several correction strategies have been proposed to correct keratometric corneal power measurement. Most are based on a comparison of corneal astigmatism and the refractive cylinder after implantation of rotationally symmetric lenses (e.g., the Abulafia-Koch correction[9]) or the correction strategies proposed by Savini[12] or Tutchenko,[18] while others use tomographic data from Scheimpflug systems to derive statistical corrections in situations where the corneal back surface cannot be derived.[19] All decompose the astigmatism into vector components using trigonometric functions (e.g., Humphrey notation[20,21]) and overlay fixed or regression-based offsets to the components to reduce or eliminate the overall trend error.

With LaHood *et al.*'s[17] total keratometry (TK) module for the IOLMaster 700 (Carl-Zeiss-Meditec, zeiss.com), which was launched to the European market in 2018, corneal back surface data is captured with a scanning SS-OCT. These data are binned to the corneal front surface data which are measured in classical fashion with telecentric keratometry to maintain distance independence of the measurement.

Key points

- The corneal back surface is a vital parameter for optical calculations, especially in the context of lens power calculation for toric implants or following refractive corneal surgery.
- The equivalent power and astigmatic vector components of the corneal back surface can be predicted using a multilinear regression model based on front surface measurements and measurements from optical biometers.
- Deep learning algorithms outperform multilinear regression models in predicting corneal back surface power, even in the case of crossed cylinders between both surfaces.

The purpose of the present study was to use a large dataset of biometric measurements with the IOLMaster 700 in a cataractous population plus the back surface measurements (TK module) to develop and train a deep learning algorithm for prediction of corneal back surface curvature from corneal front surface curvature and other biometric measures such as patient age, axial length, corneal thickness, anterior chamber depth, lens thickness and the horizontal corneal diameter. This prediction model, which could be used for standard biometers where no corneal back surface measurement is available, will be validated and compared to a multivariate linear regression model based on corneal front surface curvature data.

METHODS

Dataset for the deep learning algorithm

In total, a dataset with 48,455 measurements from the IOLMaster 700 from two clinical centres (Augenklinik Castrop, Germany and Department of Ophthalmology and Optometry, Kepler-University, Linz, Austria) was considered for this retrospective study. All biometry measurements were performed prior to cataract surgery. This study was registered at the local Ethics Committee (Ethikkommission der Ärztekammer des Saarlandes with the registration number 157/21). The data were anonymised by the source and transferred to a.csv data table using the software module for batch data export. The tables from both clinical centres were merged. Data tables were reduced to the relevant parameters required for our data analysis and finally contained measurements of corneal front surface curvature (flat meridian R1 with axis A1; steep meridian R2 with axis A2), back surface curvature (flat meridian RP1 with axis AP1; steep meridian RP2 with axis AP2), axial length (AL), CCT, phakic anterior chamber depth (ACD) measured from the corneal front apex to the lens front apex, phakic lens

thickness (LT), horizontal corneal diameter (W2W) and patient age.

Duplicate measurements of eyes, missing data or data with a 'Failed' or 'Warning' in the internal quality check of the IOLMaster 700 for keratometry, AL, CCT, ACD, LT or W2W were excluded. After checking for 'Successful' measurement for corneal front and back surface curvature data a dataset of $N = 19,553$ measurements was used for training, validation and test of our prediction algorithm. The data were transferred to MATLAB v.2019b (MathWorks, mathworks.com) for further processing.

Pre-processing of the data

Custom software was written in MATLAB 2019b. From the corneal front surface curvature data (R1/A1 and R2/A2) measured with the IOLMaster 700 the three vector components $CFSPM_{EQ}$, $CFSPM_{0°}$ and $CFSPM_{45°}$ were derived using vector decomposition according to Alpins[20]

$$CFSPM_{EQ} = 0.5 \cdot \left(\frac{n_C - 1}{R1} + \frac{n_C - 1}{R2} \right)$$

$$CFSPM_{0°} = \left(\frac{n_C - 1}{R2} - \frac{n_C - 1}{R1} \right) \cdot \cos(2 \cdot A1)$$

$$CFSPM_{45°} = \left(\frac{n_C - 1}{R2} - \frac{n_C - 1}{R1} \right) \cdot \sin(2 \cdot A1).$$

For the measured corneal back surface curvature the respective 3 vector components $CBSPM_{EQ}$, $CBSPM_{0°}$ and $CBSPM_{45°}$ were derived using

$$CBSPM_{EQ} = 0.5 \cdot \left(\frac{n_A - n_C}{RP1} + \frac{n_A - n_C}{RP2} \right)$$

$$CBSPM_{0°} = \left(\frac{n_A - n_C}{RP2} - \frac{n_A - n_C}{RP1} \right) \cdot \cos(2 \cdot AP1)$$

$$CBSPM_{45°} = \left(\frac{n_A - n_C}{RP2} - \frac{n_A - n_C}{RP1} \right) \cdot \sin(2 \cdot AP1)$$

with the refractive index $n_C = 1.376 / n_A = 1.336$ for the cornea and aqueous humour, respectively.[22]

Setup of the prediction algorithm

To identify the relevant input parameters, a stepwise fit strategy was applied. With this procedure, a stepwise linear regression model is fitted to the input data (corneal front surface power [$CFSPM_{EQ}$, $CFSPM_{0°}$ and $CFSPM_{45°}$]), AL, CCT, ACD, LT, W2W and patient age to read out the impact of the potential effect sizes. This stepwise fit begins with an initial constant model and takes forward or backward steps to add or remove variables, until a stopping criterion (maximum number of iterations: 12, significance level for a variable to be entered: 0.05) is satisfied. ACD

and lens thickness were not considered as significant effect sizes in this stepwise fit model, therefore both variables were discarded.

A feedforward shallow multi-layer multi-output neural network[23,24] was set up for predicting the corneal back surface power (output: $CBSPP_{EQ}$, $CBSPP_{0°}$ and $CBSPP_{45°}$) from the input parameters corneal front surface power ($CFSPM_{EQ}$, $CFSPM_{0°}$ and $CFSPM_{45°}$), AL, CCT, W2W and patient age. For the training function we used the Levenberg-Marquardt algorithm,[25,26] as this algorithm is known to provide good performance in terms of convergence and stability. Based on the squared prediction error derived from the three vector components of the measured and the predicted back surface power values

$$sPE = \frac{1}{3} \cdot \left(\left(CBSPP_{EQ} - CBSPM_{EQ} \right)^2 + \left(CBSPP_{0°} - CBSPM_{0°} \right)^2 + \left(CBSPP_{0°} - CBSPM_{0°} \right)^2 \right)$$

optimisation was performed in terms of minimizing the mean squared prediction error, which refers to a metric for performance P of the prediction:

$$msPE = \frac{\sum_N sPE}{N}.$$

In a preconditioning step we tested several options using the entire dataset with several choices for the number of hidden layers (1/2/3/4 hidden layers) and 1 to 25 neurons per layer with a maximum number of 50 iterations (epochs) for optimisation in order to form an impression of the required number of layers and the number of neurons in our perceptron. *Figure 1* shows the performance of the feedforward network for some selected combinations of hidden layers 1 to 4 and number of neurons per layer of 1, 2, 4, 8, and 16 using the entire dataset for training with the cumulative histograms of the squared prediction errors. From the graphs we see that the squared prediction error *sPE* becomes systematically smaller with an increasing number of neurons and increasing the number of hidden layers. However, in contrast, the complexity of the network increases rapidly with the number of hidden layers. As we noticed a large improvement only from 1 to 2 hidden layers and a very small improvement from 2 to 3 or 3 to 4 hidden layers, we decided to use 2 hidden layers in our final model. For the number of neurons per layer the behaviour is similar; there is a large improvement from 1 to 2, from 2 to 4 and from 4 to 8 neurons, but with increasing numbers of neurons the performance only improves marginally. However, an increasing number of neurons per layer makes the perceptron structure much more complex. Therefore, we decided to use 12 neurons per hidden layer in our final model as a compromise between performance and complexity.

In the next step, the dataset with $N = 19,553$ measurements was divided using a random selection into a training
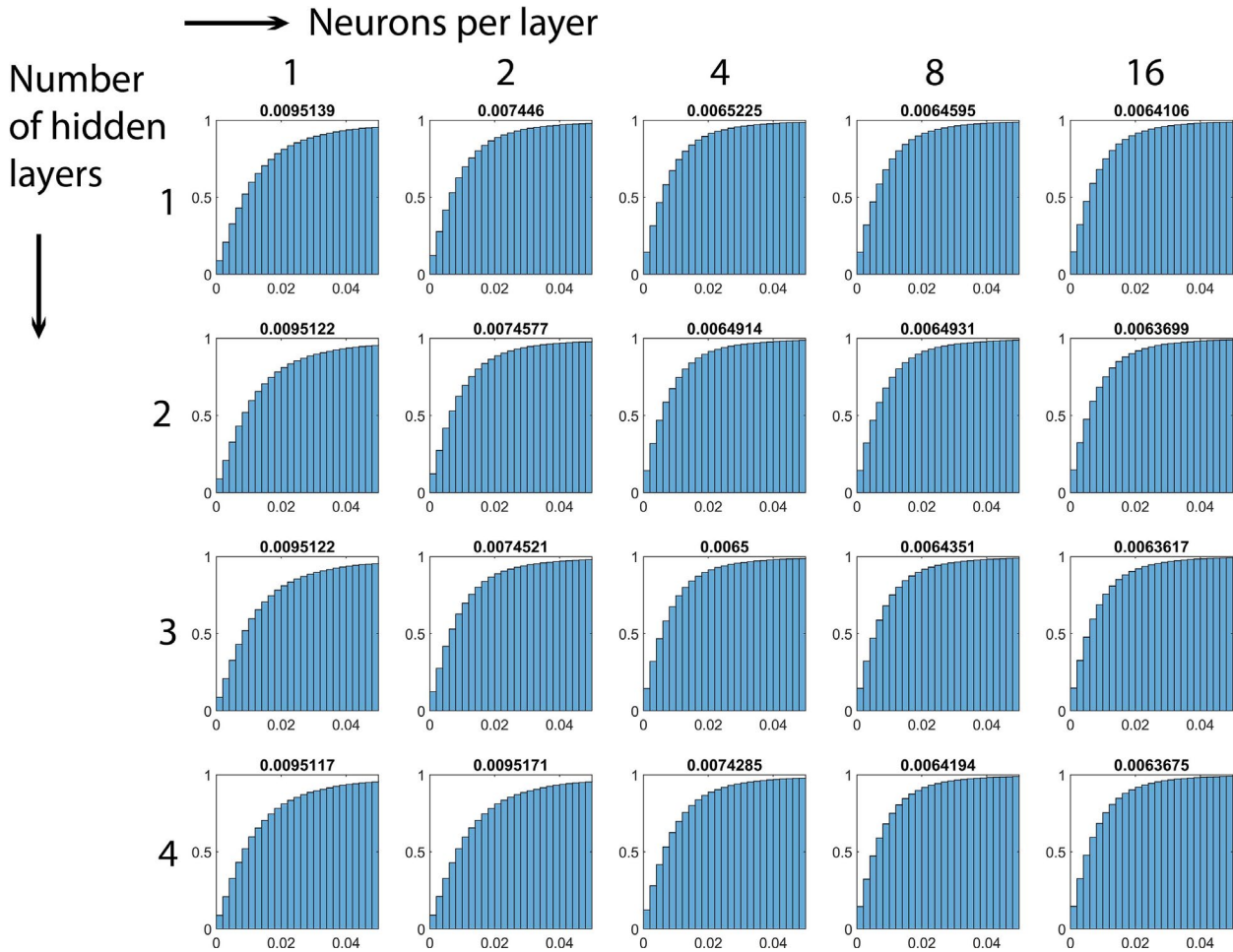
FIGURE 1 The result of the preconditioning to determine the proper number of hidden layers and number of neurons per layer. The figure displays a series of cumulative histograms of the squared prediction error for variations of number of neurons per layer (to the right, 1st column: 1 neuron per layer, 2nd column: 2 neurons per layer, 3rd column: 4 neurons per layer, 4th column: 8 neurons per layer, and 5th column: 16 neurons per layer) and number of hidden layers (1st row: 1 hidden layer to 4th row: 4 hidden layers). All histograms consider a range for the squared prediction error between 0 and 0.05 dpt^2. For comparability, all calculations in this preconditioning step are performed with 50 epochs

set (70%, N = 13,687), a validation set (N = 2933) and a test set (N = 2933).[23] The neural network was trained with the training dataset and later validated with the validation dataset. A final check was performed using the N = 2933 test dataset.

For reference we defined the corneal back surface curvature from a fixed ratio of front to back surface radius based on the Gullstrand schematic model eye (7.7 mm/6.8 mm) with the three vector components $CBSPG_{EQ}$ = 6.8/7.7·$CFSPM_{EQ}$, $CBSPG_{0°}$ = 6.8/7.7·$CFSPM_{0°}$ and $CBSPG_{45°}$ = 6.8/7.7·$CFSPM_{45°}$, respectively. In addition, we defined a multivariate linear regression model (with a 3×3 transformation matrix and a 3×1 intercept vector) which uses the three vector components $CFSPM_{EQ}$, $CFSPM_{0°}$ and $CFSPM_{45°}$ as input values to predict the three vector components $CBSPmv_{EQ}$, $CBSPmv_{0°}$ and $CBSPmv_{45°}$ as output parameters. For a direct comparison of the prediction performance of the neural network based setting and the multivariate linear regression model we also implemented a smart version of a neural network,

using the same input parameters as the multivariate linear model ($CFSPM_{EQ}$, $CFSPM_{0°}$ and $CFSPM_{45°}$) to predict the three vector components $CBSPsmart_{EQ}$, $CBSPsmart_{0°}$ and $CBSPsmart_{45°}$ as output parameters. For this purpose, we did not perform a preconditioning, but instead used a neural network structure with two hidden layers, 12 neurons per layer and 16 epochs as done for the neural network based on the full set of input parameters. All three reference models were also validated against the corneal back surface measurements $CBSPM_{EQ}$, $CBSPM_{0°}$ and $CBSPM_{45°}$ in terms of performance with the same metric (squared prediction error) using the test data.

Statistics

The input data, output data and prediction errors are shown with mean, standard deviation, median, minimum – maximum and 90% confidence intervals. The squared prediction error which shows in general a one-sided

distribution is described with median and upper 90% and upper 99% confidence intervals. For the multivariate linear prediction model we used maximum likelihood estimation with iterative ECM algorithm,[27,28] and the respective results are described with the regression coefficient matrix and LogL as the value of the log likelihood objective function after the final iteration.[28]

RESULTS

Table 1 shows the explorative statistics of the seven input parameters used to train the deep learning algorithm (AL, CCT, W2W, patient age, $CFSPM_{EQ}$, $CFSPM_{0°}$, $CFSPM_{45°}$) in terms of mean, standard deviation, median, minimum and maximum and the lower and upper limits of the 90% confidence intervals for the 19,553 measurements.

After our check for proper conditioning of the neural network with variations of number of hidden layers and number of neurons per layer, we decided to use two hidden layers with 12 neurons per layer for our final version of the prediction algorithm. With this setup (combination of number of hidden layers and number of neurons per layer) the median squared prediction error could be kept below 0.0064 D^2 (prediction error of 0.08 D, corresponding to the typical repeatability of keratometers or topographers in measuring corneal power). After splitting our dataset into training, validation and test data we checked the performance of the feedforward network. *Figure 2* (left side) shows the performance plot of our final version of the feedforward neural network with two hidden layers and 12 neurons per layer, which shows the mean squared prediction error (msPE) of the network applied to the training data, validation data and test data for variations of iterations (epochs). The vertical cyan line indicates proper results with 16 epochs, and the respective msPE for the training data, validation data and test data with 16 epochs are shown

TABLE 1 Input data for our neural network for prediction of corneal back surface power

N = 19,553	Age (years)	AL (mm)	CCT (mm)	W2W (mm)	$CFSPM_{EQ}$ (D)	$CFSPM_{0°}$ (D)	$CFSPM_{45°}$ (D)
Mean	71.11	23.68	0.55	11.98	48.82	0.19	−0.02
Standard deviation	10.44	1.34	0.04	0.40	1.70	1.13	0.68
Median	73	23.48	0.55	11.98	48.79	0.14	−0.01
Minimum	25	18.71	0.42	9.71	40.35	−9.36	−9.29
Maximum	99	31.92	0.76	13.92	55.92	8.94	5.70
5% quantile	53	21.90	0.49	11.33	46.07	−1.43	−0.99
95% quantile	85	26.12	0.61	12.64	51.63	2.02	0.94

Note: Axial length (AL), central corneal thickness (CCT), and horizontal corneal diameter W2W are directly used from the IOLMaster 700 biometer. The corneal radii and axes of the front surface curvature measured with the IOLMaster 700 are converted to vector components $CFSPM_{EQ}$, $CFSPM_{0°}$, and $CFSPM_{45°}$.
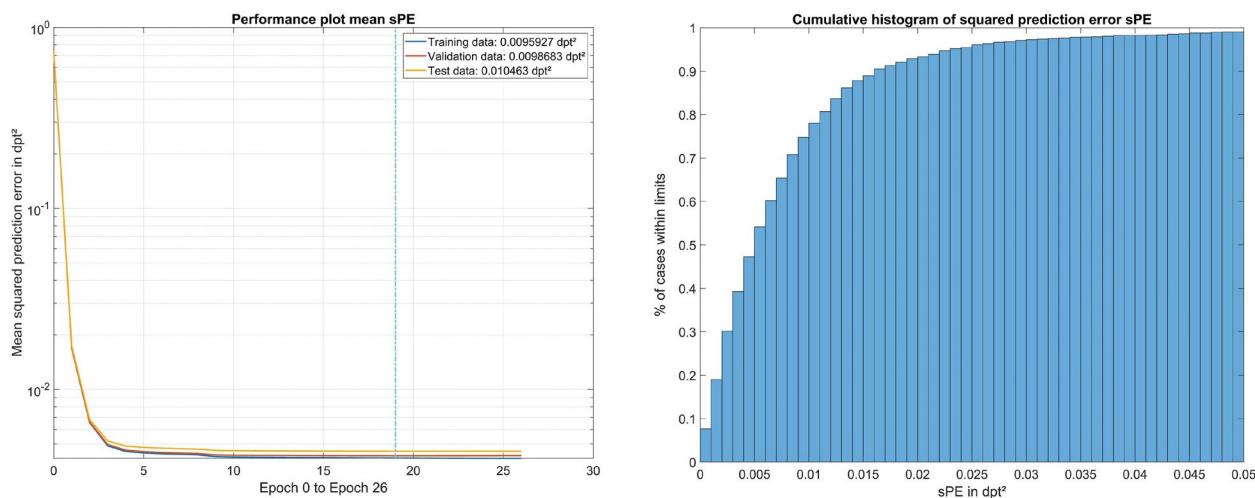
Abbreviation: D, dioptres.

FIGURE 2 Left side: Performance plot of our final version of the feedforward neural network with 2 hidden layers and 12 neurons per layer which shows the mean squared prediction error msPE of the network applied to the training data, validation data and test data for variations of iterations (epochs). The vertical cyan line indicates proper results with 16 epochs, for more iteration cycles no further improvement could be reached. The respective msPE values for 16 epochs of optimisation are shown in the legend for the training data, validation data, and test data. Right side: Cumulative histogram of the squared prediction error sPE for the N = 2933 test data using the feedforward neural network with 2 hidden layers and 12 neurons per layer optimised with 16 iterations (epochs)

in the legend. *Figure 2* (right side) displays the performance of the network with the cumulative histogram of the squared prediction error (sPE) for the $N = 2933$ test data using the feedforward neural network with two hidden layers and 12 neurons per layer optimised with 16 iterations (epochs). The median sPE is provided in the figure title.

Using the multivariate linear model for prediction of corneal back surface power vector components ($CBSPmv_{EQ}$, $CBSPmv_{0°}$, $CBSPmv_{45°}$) from corneal front surface power components measured with the IOLMaster 700 ($CFSPM_{EQ}$, $CFSPM_{0°}$, $CFSPM_{45°}$) we get a transformation matrix

$$\begin{bmatrix} CBSPmv_{EQ} \\ CBSPmv_{0°} \\ CBSPmv_{45°} \end{bmatrix} = \begin{bmatrix} 0.078 \\ -0.189 \\ 0.037 \end{bmatrix} + \begin{bmatrix} -0.137 & 0.001 & 0.002 \\ -0.001 & -0.115 & 0.000 \\ 0.001 & 0.000 & -0.120 \end{bmatrix} \cdot \begin{bmatrix} CFSPM_{EQ} \\ CFSPM_{0°} \\ CFSPM_{45°} \end{bmatrix}.$$

with a likelihood objective function value after the last iteration LogL = 5.28e4. From the coefficient matrix structure we see that the dominant elements are located in the diagonal which means that the three vector components of corneal back surface power are mostly determined by the respective component of the corneal front surface vector component, with a scaling factor of around -0.115 (for the vector component in 0°/90°) to -0.137 (for the vector component of equivalent power). In addition we can see that especially for the vector component 0°/90° there is an offset of nearly -0.2 D, whereas for the vector component in the oblique axis (45°/135°) there is only a slight offset of around 0.04 D. *Table 2* lists the values of the vector components of the corneal back surface measured with the IOLMaster 700, together with the prediction of the feedforward neural network, the data derived from a fixed ratio of front to back surface radii for both cardinal meridians extracted from the Gullstrand schematic model eye and the predicted vector components for the corneal back surface power from the multivariate linear model as described above (the respective data for the smart version neural network are not shown here). We can see from the table that for the vector component at 0° (with the rule) and 90° (against the rule), the Gullstrand model eye cannot properly represent the corneal back surface power vector components, which leads to the discrepancy between the total corneal astigmatism and keratometric corneal astigmatism based on a corneal front surface curvature measurement only. In contrast, both other prediction strategies (the neural network approach or the multivariate linear regression model) properly resample the mean value and median of all three corneal back surface vector components.

The distributions of the three vector components of the prediction error are displayed in *Figure 3* with respect to the vector components derived from the measured corneal back surface curvature $CBSPM_{EQ}$, $CBSPM_{0°}$ and $CBSPM_{45°}$. The three vector components of the neural network prediction error (left graph) show a very good performance with a narrow distribution and no systematic offset from the respective components of the measured corneal back surface

TABLE 2 Descriptive statistics of the corneal back surface power in vector components in terms of mean, standard deviation, median, minimum and maximum, 5% and 95% quantile

N = 19,553	Measured corneal back surface power (D)			Predicted corneal back surface power with neural network (D)			Corneal back surface power from Gullstrand model (D)			Corneal back surface power from multivariate regression model (D)		
	$CBSPM_{EQ}$	$CBSPM_{0°}$	$CBSPM_{45°}$	$CBSPP_{EQ}$	$CBSPP_{0°}$	$CBSPP_{45°}$	$CBSPG_{EQ}$	$CBSPG_{0°}$	$CBSPG_{45°}$	$CBSPmv_{EQ}$	$CBSPmv_{0°}$	$CBSPmv_{45°}$
Mean	−5.83	−0.23	−0.01	−5.83	−0.23	−0.01	−5.88	−0.02	0.00	−5.83	−0.23	−0.01
Standard deviation	0.24	0.16	0.11	0.21	0.12	0.08	0.21	0.14	0.08	0.21	0.12	0.07
Median	−5.83	−0.22	−0.01	−5.83	−0.23	−0.01	−5.88	−0.02	0.00	−5.83	−0.23	−0.02
Minimum	−7.12	−1.15	0.91	−6.97	−1.16	−0.81	−6.74	−1.08	−0.69	−6.68	−1.13	−0.62
Maximum	−5.00	1.28	1.18	−5.18	1.26	0.91	−4.87	1.25	1–12	−4.80	0.84	0.96
5% quantile	−6.23	−0.48	−0.18	−6.18	−0.43	−0.12	−6.22	−0.24	−0.11	−6.17	−0.42	−0.12
95% quantile	−5.45	0.00	0.15	−5.49	−0.06	0.09	−5.55	0.17	0.12	−5.50	0.06	0.09

Note: The first data block (columns 2–4) refers to the corneal back surface power measured with the IOLMaster 700, the next block (columns 5–7) to the corneal back surface power predicted with the feedforward neural network, the next block (columns 8–10) to the back surface power derived from a fixed curvature ratio (front to back surface in both cardinal meridians) extracted from the Gullstrand model eye, and last block (columns 11–13) to the prediction of corneal back surface power using a multivariate linear model with corneal front surface power vector components as predictors (the data for the smart version neural network are not shown in this table).
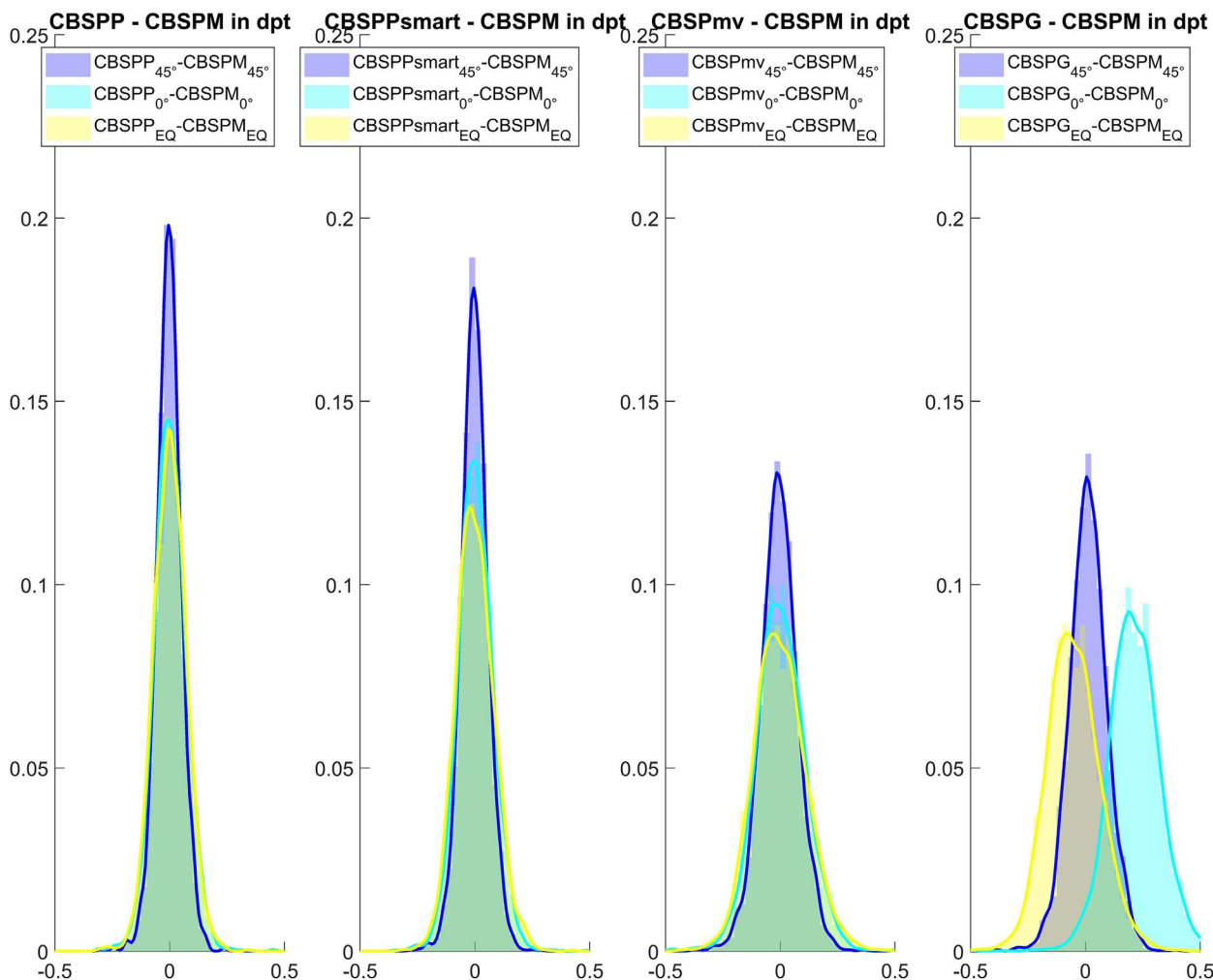
Abbreviation: D, dioptres.

FIGURE 3 Normalised histogram together with the kernel probability density distribution plot of the prediction error with respect to the vector components of the measured corneal back surface power equivalent power: CBSPMEQ, astigmatism projected to the 0°/90° meridian: CBSPM0° and astigmatism projected to the 45°/135° meridian: CBSPM45°. The 3 vector components of the neural network prediction error ([left graph] show a very good performance with a narrow distribution and no systematic offset from the respective components of the measured corneal back surface power. The smart version neural network based on the input parameters used in the multivariate linear prediction model [2nd graph from left] shows a slightly lower performance compared to the network based on all input parameters, but performs better compared to the multivariate prediction model. With the multivariate prediction model [3rd graph from left]) the distributions of the 3 vector components of the prediction error are much broader, but without a systematic offset. In contrast, with the fixed anterior to posterior curvature ratio extracted from the Gullstrand model eye (graph on the right) the distributions of the prediction error are much broader and show a systematic offset from zero mainly for the vector components equivalent power and astigmatism in 0°/45°

power. The smart version neural network with the same input parameters as used in the multivariate linear model (second graph from left) also shows a good performance, but the prediction is slightly worse compared to the neural network as shown on the left graph. With the multivariate prediction model (third graph from left) the distributions of the three vector components of the prediction error are much broader, but with no systematic offset. In contrast, with the fixed anterior to posterior curvature ratio extracted from the Gullstrand model eye (graph on the right), the distributions of the prediction error are much broader and show a systematic offset from zero for the vector components equivalent power and astigmatism in 0°/45°.

To check for any trend, *Figure 4* displays scatterplots with the prediction error using the neural network approach (in

red), the smart version of the neural network (in cyan), the multivariate linear prediction model (in blue) and the prediction using a fixed anterior to posterior corneal curvature ratio extracted from the Gullstrand model eye (in green). In the upper/middle/lower graph the situation for the vector component equivalent power/astigmatism in 0°/90°/astigmatism in 45°/135° are shown, respectively. The prediction error resulting from the neural network shows no systematic offset or effect on the respective component of the measurement. The smart version of the neural network also shows no offset or visible effect on the respective component of the measurement, but a slightly broader scatter compared to the neural network considering all seven input parameters. The prediction of the multivariate linear regression also shows no systematic offset, but an inverse effect on the respective
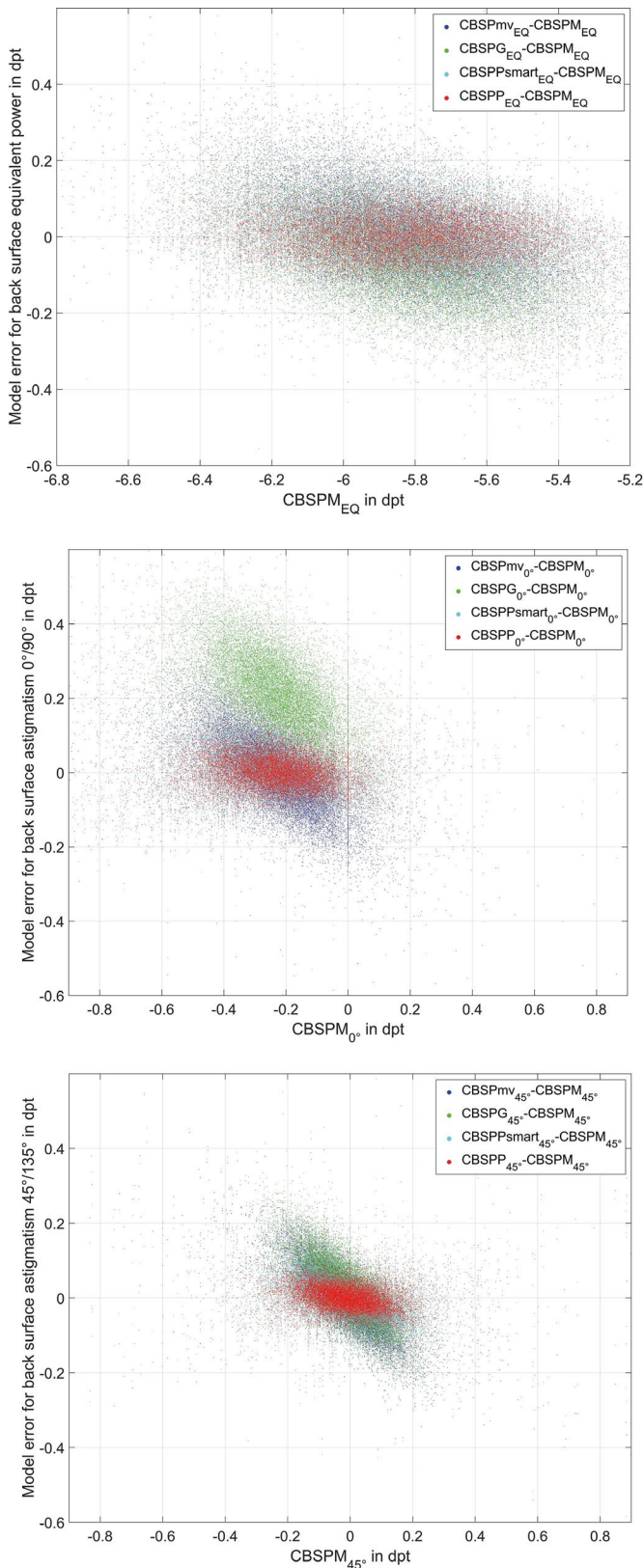
FIGURE 4 Scatterplots comparing the prediction error of four different models with the corresponding parameter as measured using the IOLMaster. In order, from top to bottom, the three plots compare the prediction error against the measured value for the three vector components: equivalent power, astigmatism in the 0°/90° orientation, and astigmatism in the 45°/135° orientation respectively. Each plot is colour coded with the colour of the plotted data points indicating the model as follows: the neural network approach with 7 effect sizes (red), the smart version neural network approach with 3 effect sizes (cyan), the multivariate linear prediction model with 3 effect sizes (blue) and the prediction using a fixed anterior to posterior corneal curvature ratio extracted from the Gullstrand model eye (green). The prediction errors resulting from the two neural network approaches show no (visible) systematic offset or trend compared to the respective component of the measurement. The prediction of the multivariate linear regression shows no vertical offset but does in each case show an inverse trend (negative gradient) against the respective measured vector component, and the prediction based on the Gullstrand model eye shows both a systematic vertical offset mainly for equivalent power and astigmatism component in 0°/90°, in addition to an inverse trend against the respective measured vector component. The scatter of the smart version neural network based model is slightly larger compared to that of the neural network based on all input parameters

DISCUSSION

It is well known that the keratometric measures, especially keratometric astigmatism, do not fully reflect corneal power.[1,10,15] Keratometers (or ophthalmometers) measure the anterior corneal curvature by projecting keratometer marks onto the cornea reflected off the tear film that are analysed by the examiner. In automatic keratometers or topographers, multiple marks or a Placido pattern with concentric rings are projected onto the cornea, and the reflected mires are evaluated. Based on a schematic model eye – in traditional keratometers, mostly the Gullstrand model eye – the power of the cornea as a meniscus lens is estimated using a keratometer refractive index, which refers to an assumed value characterised by the schematic model eye.[2] In ophthalmology, two different keratometer indices are commonly used: the Zeiss index with $n_K = 1.332$, and the Javal index with $n_K = 1.3375$. Based on the Gullstrand model eye, the Zeiss index describes the front vertex power of the model, while the Javal index represents the back vertex power. However in general, such a conversion from corneal front surface curvature to corneal power is not valid, as the corneal back surface is not in a fixed proportion to the front surface, and corneal thickness may vary.[2]

Javal's rule describes the discrepancy between keratometric astigmatism and the refractive cylinder, and this discrepancy might be due to the effect of corneal back surface curvature or lenticular astigmatism.[14,16] In the last two decades, many attempts have been made to measure the corneal back surface curvature using tomography rather than estimating the effect. Several slit projection systems fulfilling the Scheimpflug measurement condition or otherwise were launched to market that allowed the examiner to look behind the corneal front surface. In the last decade, the development of swept source OCT has made high resolution three-dimensional measurement of the anterior eye

component of the measurement, and the prediction based on the Gullstrand model eye shows both a systematic offset for equivalent power and astigmatism component in 0°/90° as well as an inverse effect in the respective component of the corneal back surface measurement.

segment possible and the corneal back surface can be measured directly.[1,7,8] Especially in the case of biometry prior to cataract surgery with implantation of toric lenses, which has gained popularity in the last two decades, the effect of corneal back surface astigmatism is highly relevant to achieve optimal refractive results after surgery. Therefore, several prediction models have been proposed,[3,4,9,10,12] either adjusting the keratometric measurement with a fixed offset or based on regression analysis using the vector components of the keratometric astigmatism and in some cases considering the orientation of corneal astigmatism before surgery (i.e., with the rule, oblique or against the rule).

Since 2018, a biometer has become commercially available which allows measurement of corneal thickness and corneal back surface curvature in addition to classical keratometry.[17] As the corneal back surface curvature can be measured directly with these biometers, such prediction models for the contribution of corneal back surface astigmatism to the total astigmatism should be based on the measurement instead of using indirect prediction strategies, e.g., using keratometry and refraction data after cataract surgery with implantation of a rotationally symmetric or toric intraocular lens.

Based on a large dataset of biometric data in a population prior to cataract surgery, corneal back surface measurements were used to set up a prediction model which estimates corneal back surface power (in vector components) from the corneal front surface power (in vector components) and several distances within the eye, plus the patient age. A deep learning algorithm with a feedforward neural network[23,24] with three output parameters (predictions of vector components of the corneal back surface power) from the input parameters patient age, AL, CCT, W2W and the three vector components of the corneal front surface power was set up and trained. The potential input parameters ACD and LT were discarded as a stepwise linear regression fit prior to setting up the model did not show a significant improvement with these variables included. A smart version of the neural network was set up using the same input parameters as the multivariate linear prediction model in order to make a direct comparison to the multivariate model. The entire dataset was split into training, validation and test data to make cross-validation and to avoid overfitting of the algorithm. Design parameters such as number of hidden layers or number of neurons per layer were evaluated before the final design of the algorithm was defined. The mean squared prediction error as the Euclidian norm of the prediction errors of the three vector components was defined as a metric for checking the performance.

The results of the neural network based algorithm (and the corresponding smart version) were compared to the respective results of a multivariate maximum likelihood linear regression algorithm which was set up as an iterative ECM algorithm optimisation[27,28] based on the vector components of the corneal front surface power. In addition, the vector components of the corneal back surface were derived from a back surface model based on a fixed front to back surface curvature ratio according to the Gullstrand schematic model eye, in the same way it is used for extracting a keratometer index.[2,21]

Both deep learning algorithms show a superior performance compared to the multivariate regression model or the prediction based on the fixed curvature ratio. However, the neural network based on all input parameters shows a better performance compared to the smart version of the algorithm, indicating that considering additional parameters beside the corneal front surface vector components (i.e., patient age and additional distances in the eye) improves the prediction of corneal back surface curvature. First, both neural networks based algorithm show no systematic offset in the prediction for all three vector components, which is the same as the multivariate linear prediction algorithm. In contrast, the prediction based on the fixed corneal front to back surface curvature ratio shows a systematic offset for all three vector components, mostly for the equivalent power and the astigmatism at 0°/90°. Second, the neural network based algorithms show a narrow distribution of all vector components of the prediction error, in contrast to the multivariate linear model or that based on the fixed ratio of corneal front to back surface curvature as shown in *Figure 3*. Third, the neural network based algorithms shows no trend error for any of the vector components of the prediction error versus the respective vector components of the measured corneal back surface power which is shown in *Figure 4*. In contrast, the multivariate linear prediction algorithm based on the vector components of the corneal front surface curvature measurements, and even more the model based on a fixed corneal front to back surface curvature ratio, shows a systematic inverse correlation between the prediction error and the respective vector component of the measured corneal back surface power.

CONCLUSION

In conclusion, the deep learning model derived here could be used in the clinical setting to predict corneal back surface power vector components from the power vector components of the corneal front surface measured with keratometry, corneal topography or a plugin-in keratometer in a biometer together with biometric data such as axial length, central corneal thickness, horizontal corneal diameter available from newer generation biometer models and the patient's age. This means that all required data are normally available in a modern cataract surgery setting to feed this neural network algorithm in order to make a proper prediction of the corneal back surface power in situations where a corneal back surface measurement is unavailable. Assuming that the measurement data of corneal back surface curvature of the device used in this study to set up our prediction model are reliable, then our prediction algorithm outperforms a multivariate linear prediction based on corneal front surface curvature data and, even more, a model based on a fixed ratio of corneal front to back surface curvature as used with keratometers when the conversion of corneal front surface curvature to corneal power is performed using a keratometer refractive index. As the neural network based prediction shows superior results compared with the multivariate model, based on

corneal front surface measurements only, this implies that there are other biometric measures (considered in our neural network approach) which systematically affect corneal back surface curvature.

CONFLICT OF INTEREST
The authors report no conflicts of interest and have no proprietary interest in any of the materials mentioned in this article.

AUTHOR CONTRIBUTIONS
Achim Langenbucher: Conceptualization (equal); Formal analysis (equal); Investigation (equal); Methodology (equal); Software (equal); Visualization (equal); Writing-original draft (equal); Writing-review & editing (equal). **Nóra Szentmáry:** Data curation (equal); Formal analysis (equal); Investigation (equal); Project administration (equal); Supervision (equal); Validation (equal). **Alan Cayless:** Formal analysis (equal); Validation (equal); Writing-original draft (equal); Writing-review & editing (equal). **Johannes Weisensee:** Conceptualization (equal); Data curation (equal); Formal analysis (equal); Resources (equal). **Jascha Wendelstein:** Conceptualization (equal); Data curation (equal); Methodology (equal); Visualization (equal). **Peter Hoffmann:** Data curation (equal); Methodology (equal); Project administration (equal); Resources (equal); Supervision (equal); Writing-review & editing (equal).

ORCID
Achim Langenbucher https://orcid.org/0000-0001-9175-6177
Nóra Szentmáry https://orcid.org/0000-0001-8019-1481
Jascha Wendelstein https://orcid.org/0000-0003-4145-2559

REFERENCES
1. LaHood BR, Goggin M, Esterman A. Assessing the likely effect of posterior corneal curvature on toric IOL calculation for IOLs of 2.50 D or greater cylinder power. *J Refract Surg* 2017;33:730–734.
2. Langenbucher A, Eberwein P, Fabian E, Szentmáry N, Weisensee J. Rückrechnung des Keratometerindex – Welcher Wert wäre bei der Kataraktchirurgie richtig gewesen? [Back-calculation of the keratometer index-Which value would have been correct in cataract surgery?] *Der Ophthalmologe*. 2021;118:356–366.
3. Goggin M, van Zyl L, Caputo S, Esterman A. Outcome of adjustment for posterior corneal curvature in toric intraocular lens calculation and selection. *J Cataract Refract Surg* 2016;42:1441–1448.
4. Goggin M, Zamora-Alejo K, Esterman A, van Zyl L. Adjustment of anterior corneal astigmatism values to incorporate the likely effect of posterior corneal curvature for toric intraocular lens calculation. *J Refract Surg* 2015;31:98–102.
5. Reitblat O, Levy A, Kleinmann G, Abulafia A, Assia EI. Effect of posterior corneal astigmatism on power calculation and alignment of toric intraocular lenses: comparison of methodologies. *J Cataract Refract Surg* 2016;42:217–225.
6. Chen YA, Hirnschall N, Findl O. Evaluation of 2 new optical biometry devices and comparison with the current gold standard biometer. *J Cataract Refract Surg* 2011;37:513–517.
7. Fişuş AD, Hirnschall ND, Findl O. Comparison of two swept-source optical coherence tomography-based biometry devices. *J Cataract Refract Surg* 2021;47:87–92.
8. Fişuş AD, Hirnschall ND, Ruiss M, et al. Repeatability of two swept-source optical coherence tomography biometers and one optical low coherence reflectometry biometer. *J Cataract Refract Surg* 2021;47:1302–1307.
9. Abulafia A, Koch DD, Wang L, et al. New regression formula for toric intraocular lens calculations. *J Cataract Refract Surg* 2016;42:663–671.
10. Hoffmann PC, Abraham M, Hirnschall N, Findl O. Prediction of residual astigmatism after cataract surgery using swept source fourier domain optical coherence tomography. *Curr Eye Res* 2014;39:1178–1186.
11. Nakano S, Iida M, Hasegawa Y, Hiraoka T, Oshika T. Influence of posterior corneal astigmatism on the outcomes of toric intraocular lens implantation in eyes with oblique astigmatism. *Jpn J Ophthalmol* 2021;65:288–294.
12. Savini G, Næser K, Schiano-Lomoriello D, Ducoli P. Optimized keratometry and total corneal astigmatism for toric intraocular lens calculation. *J Cataract Refract Surg* 2017;43:1140–1148.
13. Mohammadi SF, Khorrami-Nejad M, Hamidirad M. Posterior corneal astigmatism: a review article. *Clin Optom* 2019;11:85–96.
14. Elliott M, Callender MG, Elliott DB. Accuracy of Javal's rule in the determination of spectacle astigmatism. *Optom Vis Sci* 1994;71:23–26.
15. Jaffe NS, Clayman HM. The pathophysiology of corneal astigmatism after cataract extraction. *Trans Am Acad Ophthalmol Otolaryngol* 1975;79:OP615–OP630.
16. Grosvenor T, Quintero S, Perrigin DM. Predicting refractive astigmatism: a suggested simplification of Javal's rule. *Am J Optom Physiol Opt* 1988;65:292–297.
17. LaHood BR, Goggin M, Beheregaray S, Andrew NH, Esterman A. Comparing total keratometry measurement on the IOLMaster 700 with goggin nomogram adjusted anterior keratometry. *J Refract Surg* 2018;34:521–526.
18. Tutchenko L, Patel S, Voytsekhivskyy O, Skovron M, Horak O. The impact of changes in corneal back surface astigmatism on the residual astigmatic refractive error following routine uncomplicated phacoemulsification. *J Ophthalmol* 2020;2020:1–10.
19. Olsen T, Jeppesen P. Ray-tracing analysis of the corneal power from Scheimpflug data. *J Refract Surg* 2018;34:45–50.
20. Alpins NA, Goggin M. Practical astigmatism analysis for refractive outcomes in cataract and refractive surgery. *Surv Ophthalmol* 2004;49:109–122.
21. Langenbucher A, Eppig T, Schröder S, Cayless A, Szentmáry N. Corneal back surface power – interpreting keratometer readings and what predictions can tell us. *Z Med Phys* 2021;31:89–93.
22. Liou HL, Brennan NA. Anatomically accurate, finite model eye for optical modeling. *J Opt Soc Am A* 1997;14:1684–1695.
23. Schmidhuber J. Deep learning in neural networks: an overview. *Neural Netw* 2015;61:85–117.
24. Zell A. Simulation neuronaler netze [Simulation of neural networks]. 1st ed. Boston, MA: Addison-Wesley; 1994. p. 73.
25. Levenberg K. A Method for the solution of certain problems in least squares. *Quart Appl Math* 1944;2:164–168.
26. Marquardt D. An algorithm for least-squares estimation of nonlinear parameters. *SIAM J Appl Math* 1963;11:431–441.
27. Meng XL, Xiao L, Rubin DB. Maximum likelihood estimation via the ECM algorithm. *Biometrika* 1993;80:267–278.
28. Sexton J, Swensen AR. ECM algorithms that converge at the rate of EM. *Biometrika* 2000;87:651–662.